IEEE Photonics Journal
An IEEE Photonics Society Publication

Open Access

Optical Coherence Tomography With Gapped Spectrum

Volume 11, Number 2, April 2019

Nanshuo Wang
Xinyu Liu
Xiaojun Yu
Si Chen
Shi Chen
Linbo Liu

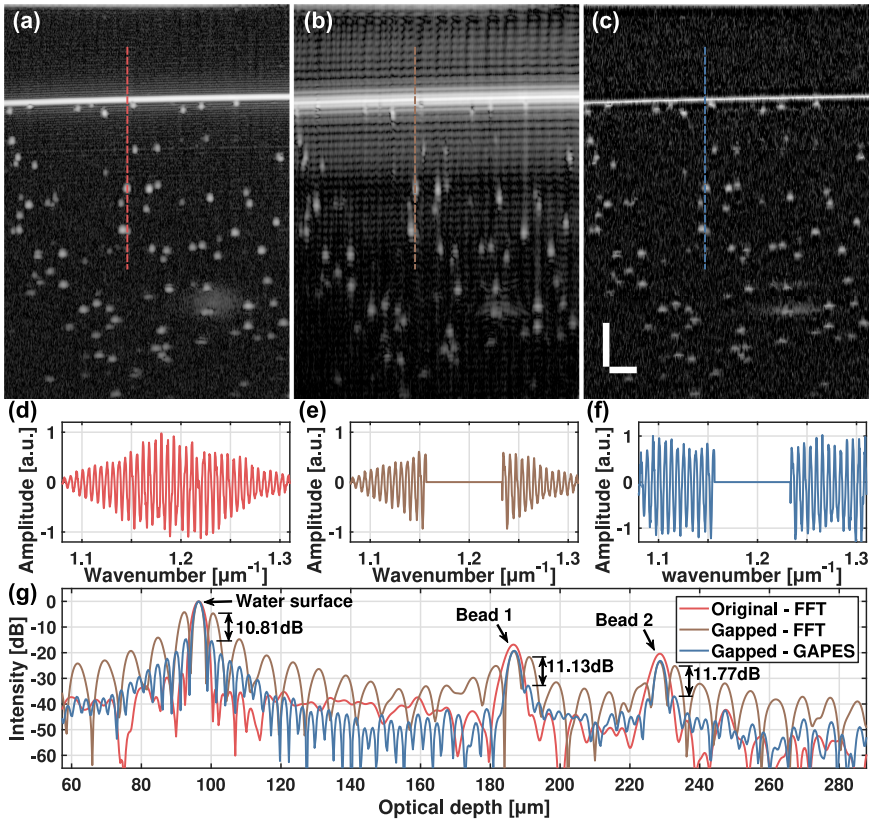

DOI: 10.1109/JPHOT.2019.2897607
1943-0655 © 2019 IEEE

Optical Coherence Tomography With Gapped Spectrum

Nanshuo Wang [1], Xinyu Liu,[1] Xiaojun Yu [2], Si Chen,[1] Shi Chen,[1] and Linbo Liu [1,3]

[1]School of Electrical and Electronic Engineering, Nanyang Technological University, Singapore 639798
[2]School of Automation, Northwestern Polytechnical University, Xi'an 710072, China
[3]School of Chemical and Biomedical Engineering, Nanyang Technological University, Singapore 637459

DOI:10.1109/JPHOT.2019.2897607

Manuscript received December 4, 2018; revised January 29, 2019; accepted January 31, 2019. Date of publication February 5, 2019; date of current version March 1, 2019. This work was supported in part by the National Research Foundation Singapore under Grant NRF-CRP13-2014-05, in part by the National Medical Research Council Singapore under Grant NMRC/CBRG/0036/2013, in part by the Ministry of Education Singapore under Grant MOE2013-T2-2-107, and in part by the NTU-AIT-MUV program in advanced biomedical imaging under Grant NAM/15005. Corresponding author: Linbo Liu (e-mail: liulinbo@ntu.edu.sg).

Abstract: The axial resolution of optical coherence tomography (OCT) is determined by the spectral shape and bandwidth of the detected light, which are limited by the gaps in the wavelength range of illumination, transmission, and detection. In this paper, we demonstrate that the axial resolution deteriorated by gaps in OCT spectra can be restored by adopting the gapped amplitude and phase estimation (GAPES) method. GAPES estimates the missing parts between separated spectral bands and obtains the axial profile of tissue with reduced sidelobe artifacts compared to the gapped spectra and significantly improved axial resolution over the individual bands. This technique may make it possible to combine spectrally separated sources and detectors to improve axial resolution in OCT images.

Index Terms: Optical coherence tomography.

1. Introduction

Over the past two decades, optical coherence tomography (OCT) has become an important clinical diagnostic technique, which is able to conduct high resolution, non-invasive imaging *in vivo* [1]. OCT can provide depth-resolved three-dimensional images by the use of both confocal gating and coherence gating. In Fourier domain OCT, the axial sample scattering profiles are obtained by inverse Fourier transform of interference spectral fringes. Therefore, the axial point-spread function (PSF) is determined by the spectrum of the low coherence light source. To obtain a PSF with high resolution and insignificant sidelobes, the spectral shape of the light source should be broad and approximately Gaussian shaped [2].

However, one cannot make full use of the near infrared biological imaging window (700–1700 nm), because there exist gaps between the water transmission windows and spectra of available light sources and detectors. Availability of light sources and detectors divides nowadays OCT devices into several wavelength categories: 800 nm, 1000 nm, 1300 nm and 1500 nm [3], [4]. For example, neither Si-based cameras nor InGaAs-based cameras have acceptable response over 900–980 nm. To make things worse, detection efficiency within this spectral band

is further degraded by the absorption peak of water at around 970 nm. An OCT system with gapped spectrum cannot provide high-quality images because inverse Fourier transform of spectra with 'gaps' would result in significant sidelobe artifacts which compromise the axial imaging performance [2].

Recently, several methods, rather than inverse Fourier transform, were proposed to retrieve the depth scattering profiles of the sample, such as the maximum entropy method [5], the algebraic reconstruction [6], and autoregressive spectral estimation methods [7], [8]. To make use of a gapped source spectrum, the straightforward idea is to apply a gapped data estimation method to retrieve the depth profiles.

Studies were conducted on the gapped data estimation problem, initially in the field of astronomy and radar, where continuous measurement was difficult because of environmental restrictions [9]–[11]. Collected data was always alternated with gaps. Huge artifacts would contaminate the spectrum if traditional spectral analysis was directly applied. Many of the data based algorithms, such as least-squares estimation [12], polynomial interpolation [13] and trigonometric polynomial interpolation [14], use the data changing tendency, or derivative, to estimate the missing data. However, these methods are applicable only when tiny gaps are scattered throughout the data sequence, in other words, can only be applied to the 'unevenly sampled data' case. In our case where there exists one big gap, the spectrum-based estimation algorithms would give more satisfying results.

To address 'big gaps' in a data sequence, Fahlman and Ulrych iteratively used the maximum entropy method to predict the missing content [15]. Brown *et al.* proposed a modification of Fahlman and Ulrych's method where the data was bandpass filtered before AR (autoregressive) model fitting process. Also, an oversampled version of the time series was generated aiming to solve the insufficient AR coefficients problem [16]. Broersen *et al.* presented an approximate maximum likelihood method which made use of only a limited part of previous data to estimate the likelihood and was usable even if less than 10% of the data was available [17].

Most of the methods are parametric methods based on the assumption that the process through which the data is acquired satisfies a certain parametric model. However, in terms of the OCT fringe data, it is difficult to determine which model, if there is one at all, can be fitted in. Stoica *et al.* proposed a non-parametric method, termed gapped data amplitude and phase estimation (GAPES) [18]. Without any presuppositions of the data acquiring process, GAPES can be applied in cases where a specific model cannot be derived. In this paper, we present to use the GAPES to estimate the missing part between spectral bands in OCT spectral data and produce images with reduced artifacts and improved axial resolution.

2. Theory

GAPES uses available interferogram to estimate the missing part, thus obtains a non-gapped spectrum. With this gap-filled interferogram, an A-line profile along the axial direction of OCT images with little sidelobes can be retrieved. APES (amplitude and phase estimation) algorithm, instead of inverse FFT, is used to perform the spectral estimation of non-gapped spectra [19]. To treat the spectral gaps, GAPES iteratively find an estimation of the missing data in the gaps by inversely solving the APES result to get the estimated time domain data through least-square optimization. The general procedure of the algorithm is shown in Fig. 1.

The recorded raw interferograms must go through the regular pre-processing process: linearly k-space resampling and dispersion calibration. Before applying any gap estimation method, we reshape the fringe data sequence to be uniform in amplitude across the whole spectrum, to fulfill the condition of a wide-sense stationary random sequence. The reshaping can be implemented through pixel-by-pixel dividing the fringe to the source spectrogram. This procedure produces a stationary sequence if the system is shot-noise limited.

If the obtained interferograms $s(k)$, $(k = 0, 1, \ldots, N-1)$ does not contain any gaps, APES algorithm can be used to estimate the depth profile $\gamma(z)$. To implement APES algorithm, we define an

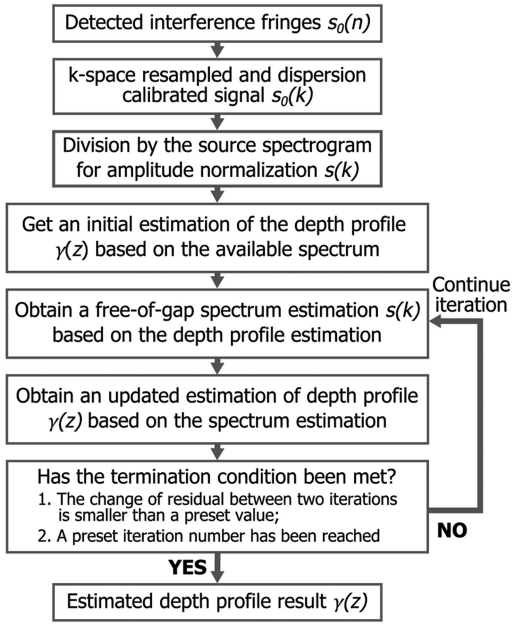

Fig. 1. The gapped-spectrum amplitude and phase estimation algorithm flowchart.

overlapping data matrix $t(k)$ based on the original interferograms $s(k)$ as follows

$$t(k) = \begin{bmatrix} s(k) \\ \cdots \\ s(k+M-1) \end{bmatrix}, (k = 0, 1, \ldots, L-1) \tag{1}$$

where $L = N - M + 1$, each row of $t(k)$ is a segment of $s(k)$ with a length of M, and adjacent elements $t(k)$ and $t(k+1)$ have $M-1$ overlapping elements. It was proved in ref [19] that a data sequence collected from a stationary stochastic process can be modeled as $\boldsymbol{h}^*(z)t(k) = \gamma(z)e^{jkz} + res$, where $\boldsymbol{h}(z)$ was the impulse response of an M-tap FIR filter, $\gamma(z)$ was the depth profile we want to resolve, and res was the residual error. The estimation of the filter bank $\hat{\boldsymbol{h}}(z)$ and the depth profile $\hat{\gamma}(z)$ can be obtained by minimizing res, expressed as

$$\min_{\gamma(z),h(z)} \sum_{k=0}^{L-1} \left| \boldsymbol{h}^*(z)\, t(k) - \gamma(z)\, e^{jkz} \right|^2 \tag{2}$$

To deal with interferograms with gaps, APES algorithm is adopted iteratively to estimate the missing part in the gaps. The first step is to give an initial guess of the depth profile and the missing data. Assuming that the missing part of the data generates the same depth profile content as the available part, an initial spectral estimation, noted as $\left\{\hat{\boldsymbol{h}}(z_i), \hat{\gamma}(z_i)\right\}$ can be obtained by directly applying APES to the available data, with the missing part set as zero. Then reversely, with the initial guess of the depth profile, an estimation of whole interferogram s_u without gaps can be obtained by solving a least square problem

$$\min_{s_u} \sum_{i=0}^{Z-1} \sum_{k=0}^{L-1} \left| \boldsymbol{h}^*(z_i)\, t(k) - \gamma(z_i)\, e^{jkz_i} \right|^2 \tag{3}$$

In this case, the interferogram s_u is the variable to be determined, while minimizing the residual error res. An updated sequence s_u without gaps can be obtained from this step, as a substitution of the original gapped interferogram. Then, by applying APES to this updated gap-filled

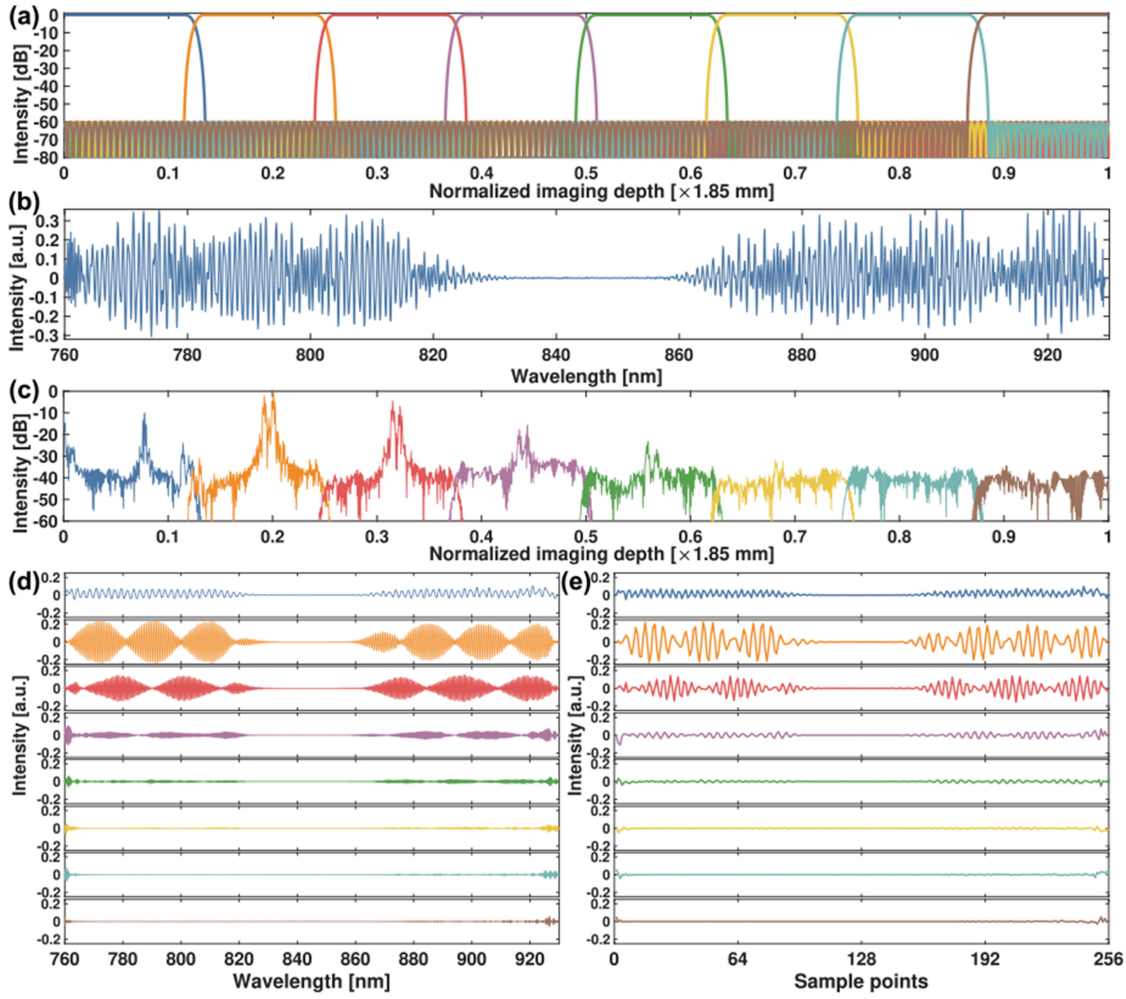

Fig. 2. The segmentation of a data sequence (a) Adjacent bandpass filters; (b) Original gapped data sequence; (c) Spectrum of filtered data; (d) Filtered data segments; (e) Spectrally shifted and down-sampled data segments.

interferogram s_u, an updated depth profile $\left\{\hat{\boldsymbol{h}}\left(z_i\right), \hat{\gamma}\left(z_i\right)\right\}$ can be obtained. With this updated depth profile, we repeat to update the interferogram estimation s_u and vice versa, until the iteration converged to the final estimation. The iteration will terminate when the change of the residual error $\sum_{i=0}^{Z-1} \sum_{k=0}^{L-1} \left|\boldsymbol{h}^*\left(z_i\right) t\left(k\right) - \gamma\left(z_i\right) e^{jkz_i}\right|^2$ between current iteration and the previous one is smaller than a threshold which is chosen according to experience and tested based on the specific applications. Though, in rare occasions, the algorithm converges slowly or even fails to converge and requires a termination forced by a preset maximum iteration number to break the loop.

In practical experiments, the computation load of the algorithm increased exponentially with the data sequence length. When the data length exceeded 1000 points, the consuming time became unacceptable. So we devised a speed-up method that divided the data sequence into 8 segments in the spatial domain and applied the algorithm individually for each short segment, followed by fusing the spectrum segments into a whole depth profile.

To segment the data sequence, we filtered the data with eight adjacent band-pass filters equally distributed along the spatial domain. These finite real filters (Fig. 2(a)) were designed to span over half of the entire spatial domain since real data sequences, such as the interference fringes, have symmetric spectral content. To illuminate the process, an A-scan fringe data sequence was shown

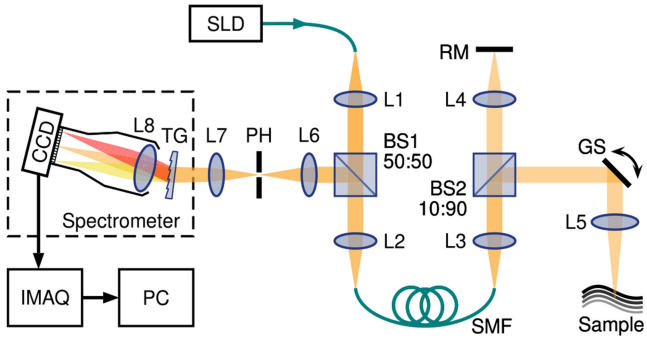

Fig. 3. Schematic of the OCT system. BS, beam splitter; GS, galvo scanners; L1-8: lenses; PH, pinhole; RM, reference mirror; SLD: superluminescent diode source; SMF, single mode fiber; TG, transmission grating; PC, personal computer; IMAQ, image acquisition board.

in Fig. 2(b) as an example, and its spatial domain transformation processed by the filters was shown in Fig. 2(c). The resultant 8 spatial domain segments were then aligned to the lowest spatial band by multiplying a frequency shifting factor $[\exp(-j\frac{2\pi(m-1)n}{8N})]$ (where $m = 1, 2, \ldots, 8$ was the index of filter, n was the index of data sequence and N was the data length). After the shifting, since the spectral information of each shifted spatial segment was constricted in the normalized spatial range $0 \sim 1/8$, we could downsample each segment with a factor of 8 without alias (shown in Fig. 2(e)). In summary, we segmented a data sequence into 8 segments each with $1/8$ of the original length.

After the segmentation, GAPES algorithm were applied to each filtered and downsampled interferogram to estimate the non-gapped depth profile. Then we shifted the depth profile segments back to their original position in the spatial domain to form the full depth profile. The segmentation dramatically improved the processing speed of GAPES. In the case of a 1024 points interferogram, the processing speed was improved by a factor of 350 (running time reduced from 25800 s to 72 s).

3. Experiments and Results

To verify the efficacy of GAPES method for gapped OCT data restoration, we developed a home-made spectral domain OCT system. A stack of glass slides was imaged to characterize the axial PSF estimation over the entire imaging depth. To compare the biological tissue images obtained by the gapped spectrum and the full spectrum, we imaged beads solution and a fresh rat cornea sample with full spectrum and numerically created gapped spectrum.

As shown in Fig. 3, a free-space spectral domain OCT setup based on Michelson interferometer was constructed. A superluminescent diode array (SLD, model: Superlum T-850-HP) with a center wavelength of 850 nm and a total bandwidth of 165 nm was used as the illumination source. A 10:90 non-polarizing beam splitter (BS029, Thorlabs Inc.) divided the beam into reference and sample arms. The two beams were focused into diffraction-limited spots by two identical focusing lenses (L4/L5: Mitutoyo Plan Apo NIR, 20 $\times$, NA 0.4). In the sample arm, two galvo mirrors (GVSM002/M, Thorlabs Inc.) were used to scan the spot in orthogonal lateral directions. The backscattered light from the sample and reflected light from the reference mirror was recombined at the beamsplitter, and guided to a home-made spectrometer through a single mode fiber (P3-780A-FC-2, Thorlabs Inc.) and a 50:50 beam splitter (BS014, Thorlabs Inc.). A 10 μm pinhole (P10S, Thorlabs Inc.) was used to reject stray light from entering the spectrometer. After being dispersed by a transmission grating (1200 lines/mm, 840 nm, Wasatch Photonics Inc.) and focused by a camera lens (Nikon AF-S 85 mm f/1.8D), the beam was directed to the line-scan CCD (E2V, AViiVA EM4) with 2048 pixels operating at an acquisition speed of 20k A-lines per second.

The superluminescent diode array provided a spectrum with a 3 dB bandwidth from 760 nm to 925 nm. To create a gap in the spectrum, we imaged the samples with full spectrum and set

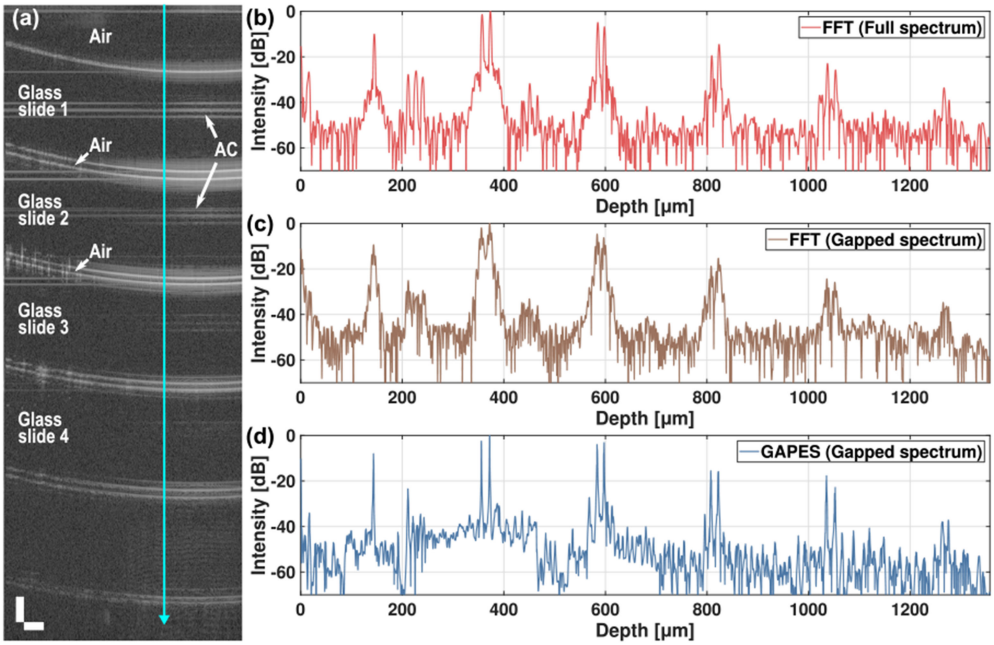

Fig. 4. Aline profiles of the glass slide stack image. (a) One frame retrieved by FFT using full spectrum light source indicating the phantom structure. The location of depth profile shown in (b–d) was indicated by blue vertical line. AC: autocorrelation artifacts. Scale bar, horizontal: 50 μm; vertical: 50 μm. (b) FFT with full spectrum. (c) FFT with gapped spectrum. (d) GAPES with the gapped spectrum.

middle $1/3$ part of acquired spectral fringes to zeros, obtaining an illuminating spectrum with two discontinued sub-bands: 760 nm–815 nm and 870 nm–925 nm.

To test the sensitivity 'roll off' and imaging depth of the gapped spectrum OCT, we imaged a glass slide stack (Fig. 4(a)), which was formed by stacking multiple glass slides together (thickness of each slice was $\sim$0.2 mm). As shown in Fig. 4, the sensitivity 'roll off' and the imaging depth was not affected by the GAPES algorithm. Comparing the full spectrum FFT depth profile (Fig. 4(b)) and the GAPES depth profile (Fig. 4(d)) it can be confirmed that the layer structure in GAPES is a representation of real sample structure. Besides, we could see significant resolution improvement and sidelobe artifacts suppression provided by the GAPES algorithm compared to the FFT result (Fig. 4(c)).

To demonstrate the performance of this method on spherical scatters which resemble biological cells, polystyrene calibration particles (80177, Fluka, diameter 2 μm) water solution was imaged (Fig. 5) with the full spectrum and a gapped spectrum with the middle 1/3 spectral data set to zeros (815 nm to 870 nm in a full spectral range from 760 nm to 925 nm). Figs. 5(a)–5(c) show images obtained from the Gaussian reshaped full spectrum (Fig. 5(d)) using conventional FFT, the Gaussian reshaped gapped spectrum using FFT (Fig. 5(e)), and the uniformly reshaped gapped spectrum (Fig. 5(f)) using GAPES, respectively. Fig. 5(g) reveals the depth profile at the location indicated by color-coded vertical lines in Figs. 5(a)–5(c). A gap in the middle of the spectrum introduced sidelobe artifacts in axial PSF, totally undermining the image quality. However, by adopting GAPES spectral estimation to retrieve the depth profile, the artifacts were suppressed by $\sim$11 dB according to the signal peaks corresponding to the water surface and beads, thereby providing image quality comparable to that of the full spectrum.

To test gapped spectrum OCT in biological tissues, we demonstrated *ex vivo* imaging on fresh rat cornea. Rat eye balls were harvested from a healthy adult female Sprague Dawley rat immediately after the disappearance of vital signs. We imaged the sample with full spectrum. To simulate a gapped spectrum, we set middle $1/3$ part of acquired spectral fringes to zeros. Figs. 6(a)–6(c)

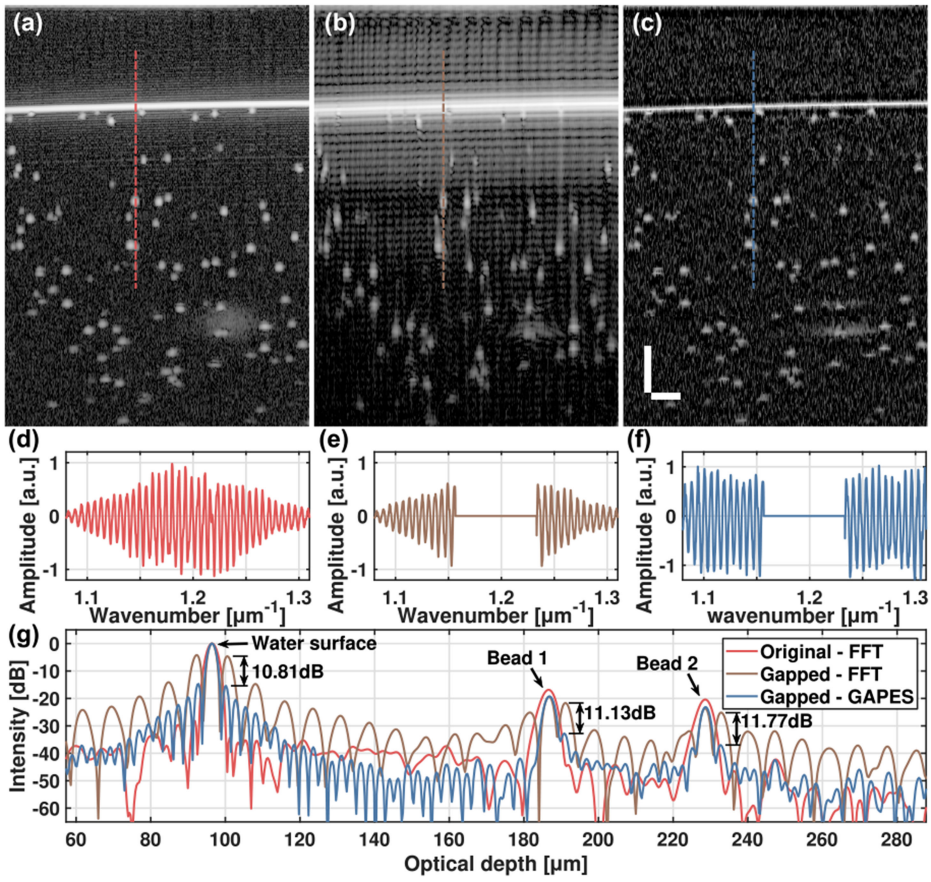

Fig. 5. Images of polystyrene calibration particles in water. (a) Full spectrum image retrieved by FFT; (b) Gapped spectrum image retrieved by FFT. (c) Gapped spectrum image retrieved by GAPES. Scale bar, horizontal: 30 μm; vertical: 50 μm. (d–f) Gaussian reshaped full spectrum (d), Gaussian reshaped gapped spectrum (e), and uniformly reshaped gapped spectrum (f) from the same A-scan after background subtraction, respectively. (g) Depth profiles at the locations indicated by the red (a), brown (b) and blue (c) vertical lines in the intensity images (a)–(c). For the peaks corresponding to water surface and beads, GAPES achieves ~11 dB sidelobe suppression comparing to direct FFT of the gapped spectrum.

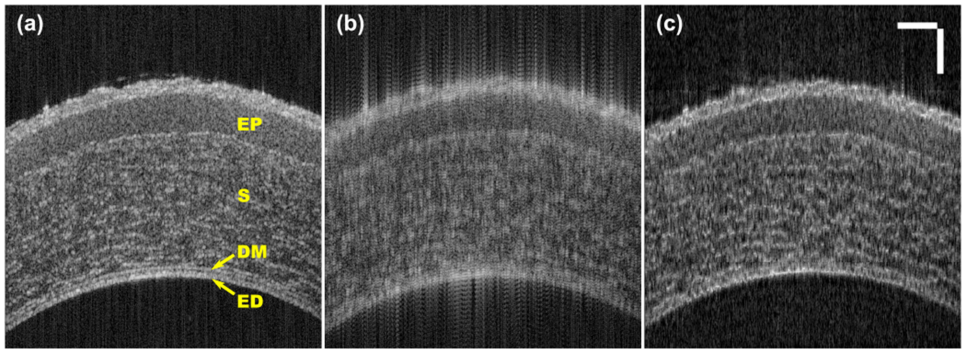

Fig. 6. Images of the rat cornea *ex vivo*. (a) Full spectrum image retrieved by FFT, (b) gapped spectrum image retrieved by FFT, and (c) gapped spectrum image retrieved by GAPES. EP: Epithelium. S: Stroma. DM: Descemet's membrane. ED: Endothelium. Scale bar, horizontal: 200 μm; vertical: 40 μm.

show the images obtained from full spectrum using conventional FFT, gapped spectrum using FFT, and gapped spectrum using GAPES, respectively. The sidelobe artifacts introduced by the spectral gap were well suppressed, and the image quality was improved in the images provided by use of GAPES (Fig. 6(c)) compared with the gaped FFT image (Fig. 6(b)).

4. Discussion and Conclusion

The estimation method was demonstrated on a SD-OCT system, however, it should have the same performance on a SS-OCT system, provided proper pre-conditioning steps such as wavenumber space remapping and dispersion calibration were completed. If two separated spectral bands are acquired by two individual detectors, after *k*-space resampling and dispersion calibration, the two sets of interference fringes should be mapped onto the same wavenumber space [20] before the gap estimation method can be adopted.

The length of the gap significantly influenced the performance of GAPES. We tested this by setting the gap lengths as 20%, 40% and 60% of the total data length, and found that the performance of GAPES decreased as the gap length increased. Larger gaps would result in more artifacts, where the speckle pattern seems like 'snakes', degrading the axial resolution and image quality. If the missing part exceeds half of the total data length, matrices in the iteration process will degenerate closely to singular matrices, making the computation of their inversion inaccurate. We tried a 70% gap length but failed because the solution collapsed to an invertible matrix. Empirically, we expected that the performance of GAPES is acceptable with a gap length no larger than 40% of the total sequence length.

Currently, there are still limitations that may hinder the practical application of this algorithm. One is the high computation load due to the large amount of matrix multiplication, inversion calculation, and iterative procedures adopted by the algorithm. We adopted an additional digital filtering and recombination procedure to speed up the computation to an acceptable level. To estimate a single A-line profile from 1024 points gapped spectrum, the computing time was about 72 seconds with six iterations running on a Xeon E5 processor computer. However, it was still not fast enough for practical clinical applications. To solve this problem, we can take advantage of the acceleration method even further, such as discarding higher spatial frequency bands for less computational load or adopting dynamically relaxed termination condition in spatial segments of less importance. In addition, the algorithm is suitable to be optimized to run on GPU or multi-core CPU for higher efficiency.

Another limitation is that the algorithm may introduce additional artifacts to the image. These artifacts turned the axial PSF to thinner peaks, thereby changing the speckle pattern to random 'snake noise' pattern, sometimes seriously blurring the image. These artifacts were reported before in the attempts of improving OCT axial resolution without broadening the light source, such as deconvolution [21] and spectral estimation [8]. We believe these artifacts are the result of the assumption that the undetectable fringes (spectral gaps or outside the source window) have the same spectral content with the known fringe data. Since OCT forms a band pass image of the sample in the axial direction [22], this assumption only stands true when the sample is made of Dirac delta functions, whose spectral content are evenly distributed in the frequency domain. Based on this assumption, the GAPES algorithm tends to turn the PSF into thinner peaks like the Dirac delta function and introduces 'snake noise' pattern into the image.

To conclude, we present, for the first time to our knowledge, how to retrieve OCT image from a gapped spectrum illuminating light source with significantly suppressed sidelobe artifacts and effective restored axial resolution using GAPES algorithm. In the OCT device, the critical component is the broadband laser source, which rolls up the cost of the whole device [23]. This method may make it possible to improve axial resolution using light sources with gapped spectrum, which is of lower cost than those of supercontinuum sources [24], [25]. What's more, this method provides a possibility to combine OCT devices in different optical bands, further improving the axial resolution.

References

[1] D. Huang *et al.*, "Optical coherence tomography," *Science*, vol. 254, no. 5035, pp. 1178–1181, 1991.
[2] R. Tripathi, N. Nassif, J. S. Nelson, B. H. Park, and J. F. de Boer, "Spectral shaping for non-Gaussian source spectra in optical coherence tomography," *Opt. Lett.*, vol. 27, no. 6, pp. 406–408, 2002.
[3] F. Spöler *et al.*, "Simultaneous dual-band ultra-high resolution optical coherence tomography," *Opt. Exp.*, vol. 15, no. 17, pp. 10 832–10 841, 2007.
[4] T. Klein and R. Huber, "High-speed OCT light sources and systems," *Biomed. Opt. Exp.*, vol. 8, no. 2, pp. 828–859, 2017.
[5] Y. Takahashi, Y. Watanabe, and M. Sato, "Application of the maximum entropy method to spectral-domain optical coherence tomography for enhancing axial resolution," *Appl. Opt.*, vol. 46, no. 22, pp. 5228–5236, 2007.
[6] H. L. Seck, Y. Zhang, and Y. C. Soh, "High resolution optical coherence tomography by ℓ 1-optimization," *Opt. Commun.*, vol. 284, no. 7, pp. 1752–1759, 2011.
[7] S. Yousefi, J. Qin, and R. K. Wang, "Super-resolution spectral estimation of optical micro-angiography for quantifying blood flow within microcirculatory tissue beds in vivo," *Biomed. Opt. Exp.*, vol. 4, no. 7, pp. 1214–1228, 2013.
[8] X. Liu, S. Chen, D. Cui, X. Yu, and L. Liu, "Spectral estimation optical coherence tomography for axial super-resolution," *Opt. Exp.*, vol. 23, no. 20, pp. 26 521–26 532, 2015.
[9] N. R. Lomb, "Least-squares frequency analysis of unequally spaced data," *Astrophys. Space Sci.*, vol. 39, no. 2, pp. 447–462, 1976.
[10] J. D. Scargle, "Studies in astronomical time series analysis. ii-statistical aspects of spectral analysis of unevenly spaced data," *Astrophys. J.*, vol. 263, pp. 835–853, 1982.
[11] G. B. Rybicki and W. H. Press, "Interpolation, realization, and reconstruction of noisy, irregularly sampled data," *Astrophys. J.*, vol. 398, pp. 169–176, 1992.
[12] F. J. Barning, "The numerical analysis of the light-curve of 12 lacertae," *Bull. Astron. Inst. Netherlands*, vol. 17, 1963, Art. no. 22.
[13] E. Groth, "The pulse shape of the crab nebula pulsar, PSR 0531+ 21, in the V and I bands," *Astrophys. J.*, vol. 200, pp. 278–280, 1975.
[14] H.-M. Adorf, "Reconstructing a one-dimensional signal from irregular samples," in *Proc. Eur. Southern Observ. Conf. Workshop*, vol. 47, 1993, pp. 191–196.
[15] G. Fahlman and T. Ulrych, "A new method for estimating the power spectrum of gapped data," *Monthly Notices Roy. Astron. Soc.*, vol. 199, no. 1, pp. 53–65, 1982.
[16] T. M. Brown and J. Christensen-Dalsgaard, "A technique for estimating complicated power spectra from time series with gaps," *Astrophys. J.*, vol. 349, pp. 667–674, 1990.
[17] P. M. Broersen, S. De Waele, and R. Bos, "Application of autoregressive spectral analysis to missing data problems," *IEEE Trans. Instrum. Meas.*, vol. 53, no. 4, pp. 981–986, Aug. 2004.
[18] P. Stoica, E. G. Larsson, and J. Li, "Adaptive filter-bank approach to restoration and spectral analysis of gapped data," *Astron. J.*, vol. 120, no. 4, 2000, Art. no. 2163.
[19] J. Li and P. Stoica, "An adaptive filtering approach to spectral estimation and SAR imaging," *IEEE Trans. Signal Process.*, vol. 44, no. 6, pp. 1469–1484, Jun. 1996.
[20] D. Cui *et al.*, "Dual spectrometer system with spectral compounding for 1-μm optical coherence tomography in vivo," *Opt. Lett.*, vol. 39, no. 23, pp. 6727–6730, 2014.
[21] E. Bousi and C. Pitris, "Axial resolution improvement by modulated deconvolution in fourier domain optical coherence tomography," *J. Biomed. Opt.*, vol. 17, no. 7, 2012, Art. no. 071307.
[22] Y. Pan, R. Birngruber, J. Rosperich, and R. Engelhardt, "Low-coherence optical tomography in turbid tissue: Theoretical analysis," *Appl. Opt.*, vol. 34, no. 28, pp. 6564–6574, 1995.
[23] A. Unterhuber *et al.*, "Compact, low-cost ti: Al 2 o 3 laser for in vivo ultrahigh-resolution optical coherence tomography," *Opt. Lett.*, vol. 28, no. 11, pp. 905–907, 2003.
[24] L. Liu *et al.*, "Imaging the subcellular structure of human coronary atherosclerosis using micro-optical coherence tomography," *Nature Med.*, vol. 17, no. 8, pp. 1010–1014, 2011.
[25] L. Liu *et al.*, "Method for quantitative study of airway functional microanatomy using micro-optical coherence tomography," *PloS one*, vol. 8, no. 1, 2013, Art. no. e54473.